Atmospheric
Chemistry
and Physics
Discussions

GOMOS data characterization and error estimation

J. Tamminen[1], E. Kyrölä[1], V. F. Sofieva[1], M. Laine[1], J.-L. Bertaux[2],
A. Hauchecorne[2], F. Dalaudier[2], D. Fussen[3], F. Vanhellemont[3],
O. Fanton-d'Andon[4], G. Barrot[4], A. Mangin[4], M. Guirlet[4], L. Blanot[4], T. Fehr[5],
L. Saavedra de Miguel[5], and R. Fraisse[6]

[1]Finnish Meteorological Institute, Earth Observation, Helsinki, Finland
[2]Service d'Aeronomie, Paris, France
[3]BIRA-IASB, Brussels, Belgium
[4]ACRI ST, Sophia Antipolis, France
[5]ESA-ESRIN, Italy
[6]EADS-Astrium, Toulouse, France

Abstract

The Global Ozone Monitoring by Occultation of Stars (GOMOS) instrument uses stellar occultation technique for monitoring ozone and other trace gases in the stratosphere and mesosphere. The self-calibrating measurement principle of GOMOS together with a relatively simple data retrieval where only minimal use of a priori data is required, provides excellent possibilities for long term monitoring of atmospheric composition.

GOMOS uses about 180 brightest stars as the light source. Depending on the individual spectral characteristics of the stars, the signal-to-noise ratio of GOMOS is changing from star to star, resulting also varying accuracy to the retrieved profiles. We present the overview of the GOMOS data characterization and error estimation, including modeling errors, for ozone, NO_2, NO_3 and aerosol profiles. The retrieval error (precision) of the night time measurements in the stratosphere is typically 0.5–4% for ozone, about 10–20% for NO_2, 20–40% for NO_3 and 2–50% for aerosols. Mesospheric O_3, up to 100 km, can be measured with 2–10% precision. The main sources of the modeling error are the incompletely corrected atmospheric turbulence causing scintillation, inaccurate aerosol modeling, uncertainties in cross sections of the trace gases and in the atmospheric temperature. The sampling resolution of GOMOS varies depending on the measurement geometry. In the data inversion a Tikhonov-type regularization with pre-defined target resolution requirement is applied leading to 2–3 km resolution for ozone and 4 km resolution for other trace gases.

1 Introduction

Vertical profiles of stratospheric constituents have been measured using satellite instruments since 1979 when SAGE I (Stratospheric Aerosol and Gas Experiment I), the first instrument of the successful SAGE family, started to operate. The solar occultation technique that was used by the SAGE instruments has turned out to be a reliable way of studying the atmospheric composition and several instruments, in addition to

the SAGE series, have utilised the same technique at various wavelenght regions including ATMOS, SAM II, HALOE, POAM series, ACE-mission and SCIAMACHY. The success story of the solar occultation technique goes on and recently launched solar occultation instruments SOFIE (Solar occultation for Ice Experiment) on board AIM
5 satellite and SEE (Solar EUV Experiment) on board TIMED satellite are targeted for studying the mesospheric and thermospheric composition, respectively.

In addition to sun also stars can be used as a light source when studying the composition of the atmosphere. This was theoretically demonstrated by Hays and Roble (1968) and later also shown in practice. In 1996 US launched MSX satellite with UVISI
10 instrument on-board, which performed several stellar occultation measurements and demonstrated the potential of the technique to study globally the atmospheric composition and temperature despite that it was not designed for that particular purpose (Yee et al., 2002; Vervack et al., 2003). For a more comprehensive summary of the occultation instruments see Bertaux et al. (2010).

15 The first instrument specifically developed for studying the composition of the atmosphere by utilizing the stellar occultation technique is European Space Agency's GOMOS (Global Ozone Monitoring by Occultation of Stars) instrument on-board the Envisat satellite, launched in March 1st 2002 (Bertaux et al., 2004; Kyrölä et al., 2004; Bertaux et al., 2010). GOMOS is a ultraviolet-visible spectrometer that covers wave-
20 lengths from 250 nm to 675 nm with 1.2 nm resolution and in addition two infrared channels at 756–773 nm and 926–952 nm with 0.2 nm resolution. Two photometers that are located at blue (473–527 nm) and red (646–698 nm) measure the stellar flux through the atmosphere at a sampling frequency of 1 kHz. By August 2009 GOMOS had observed about 668 000 stellar occultations. An overview of the GOMOS instrument and
25 highlights of the measurements are given in Bertaux et al. (2010)

The stellar occultation technique shares the main advantages of the solar occultation technique that include the self-calibrated measurement principle (see Fig. 1), relatively simple inverse problem and high vertical resolution. In addition, the stellar occultation technique benefit from the multitude of the stars to obtain a good global and temporal

coverage. Compared to the solar occultation, stars are point-like sources that result in an excellent pointing information. The disadvantage compared to the solar occultation is the signal-to-noise ratio that is much lower in the stellar occultation technique.

GOMOS is following about 180 different stars while they are descending behind the Earth limb. Since the stars are different both in brightness (magnitude) and in the spectrum of the light (originating from stellar properties and surface temperature) also the data characteristics measured by GOMOS vary strongly. Even without taking the atmospheric impact into account, the signal-to-noise ratio varies strongly from star to star. In this respect, one might even consider GOMOS being a remote sensing mission that consists of 180 different instruments each having its own data characteristics.

The importance of the data characterization and the error estimation is nowadays widely recognized (see e.g., Rodgers, 2000). The further utilization of the remote sensed data, e.g., in the assimilation or in constructing time series, depends crucially on a proper error characterization. The purpose of this paper is to characterize the quality of the GOMOS night time data products. Both systematic errors and random errors are considered. The results shown here are based on estimating the impact of various assumptions that are made in the GOMOS data processing. The GOMOS Level 1b and Level 2 data processing are described in details in Kyrölä et al. (2010). A review of the geophysical validation of GOMOS data products is included in Bertaux et al. (2010).

In this paper, we characterize O_3, NO_2, NO_3 and aerosol profiles that are retrieved from GOMOS UV-VIS spectrometer data at the altitude range 10–100 km during the night time. Only dark limb (night) occultations, i.e., occultations with solar zenith angle larger than 107 deg, are considered. The bright limb occultations (i.e., made during day time) are not considered here since the data quality in these measurements is much poorer due to the strong contribution from scattered solar light. The error characterization which we describe here corresponds to official GOMOS processor IPF Version 6 data that will be available in spring 2010. Most of the results are also valid for IPF Version 5 data which is presently available. In addition, we have tried to indicate, when

necessary, the difference in IPF Version 5 and 6 data. General features of GOMOS measurements are given in Sect. 2. The propagation of the random measurement error through the retrieval steps are discussed in Sect. 3. The contribution of various modelling errors are discussed in Sect. 4. The vertical resolution is discussed in Sect. 5. The precision of the retrieved profiles varies strongly from occultation to occultation and this is discussed in Sect. 6, where we give examples of the GOMOS error estimates and discuss the valid altitude range of the profiles. Finally, we summarize the most important sources of random and systematic errors in Sect. 7.

2 GOMOS spectral measurements and their characteristics

2.1 Signal-to-noise ratio

GOMOS measures the stellar light through the atmosphere as the stars set behind the Earth limb. However, stars are not similar and this has an impact on GOMOS results as well. The most significant characteristic related to the stellar occultation technique is that the accuracy of the retrieved parameters depends strongly on the stellar properties.The measured stellar signal and further the transmission which is used as the data in the GOMOS retrievals varies strongly depending on the stellar brightness and temperature. This is illustrated in Fig. 2, where examples of the GOMOS transmission spectrum at different altitudes (10–70 km) are shown for different stars (bright and cool, bright and hot, dim and cool and dim and hot). We observe clearly that the data using dim stars are much noisier compared to using bright stars. In addition, the stellar temperature has an impact: hot stars have the maximum intensity of the radiation at UV wavelengths whereas cool stars have the maximum at the VIS wavelengths and the UV part is very noisy.

In Fig. 3 the GOMOS signal-to-noise ratio at 3 different wavelenght regions (UV and 2 visible) are shown in three cases: Sirius (the brightest star, star number 1 in GOMOS star catalogue with magnitude $M_v = -1.44$ and temperature $T = 11000$ K), bright and

cool star (star number 4, $M_v=-0.01$, $T=58\,00$ K) and dim and cool star (star number 117, $M_v=2.7$, $T=38\,00$ K). When retrieving ozone at high altitudes, above 40 km, the Hartley band (248–310 nm) is crucial and at this altitude region the hot stars provide significantly better results than the cool stars. The average SNR of GOMOS at UV around 50 km using Sirius is 130–160 whereas using cool stars ($T<6000$ K, stars 4 and 117 in Fig. 3) the SNR is close to zero. At lower altitudes, where the retrieval is most sensitive to Chappuis band at visible wavelengths both hot and cool stars are, in general, equally good. For NO_3 the situation is quite the opposite. The strongest NO_3 signal comes from visible wavelengths around 660 nm, hence the cool stars are slightly more favourable for NO_3 retrieval. Aerosols and NO_2 are retrieved mainly below 50 km using a wide spectral window and therefore the retrievals do not have significant dependence on the stellar temperature.

Statistics of the stellar characteristics in the night time occultations during years 2002–2008 are given in Table 1. The occultations are divided into nine categories depending the stellar brightness and temperature. Roughly two thirds of the occultations are performed using either hot or medium temperature stars and about half using either bright or medium brightness stars.

2.2 Spatio-temporal distribution of GOMOS measurements

2.2.1 Mission planning

As the light source GOMOS uses about 180 brightest stars with stellar magnitude brighter than 3 ($M_v<3$). As there are often several stars available simultaneously in the GOMOS field-of-view some prioritization needs to be made. The purpose of the GOMOS mission planning is to select for each orbit the optimal set of 25–40 stars that will be used for occultation measurements. About half of the occultations are made in night time. The optimization is done using several criteria, like the geographical coverage, stellar brightness and temperature, see Kyrölä and Tamminen (1999) for more details about selecting the stars.

Title Page

Abstract | Introduction

Conclusions | References

Tables | Figures

|◄ | ►|

◄ | ►

Back | Close

Full Screen / Esc

Printer-friendly Version

Interactive Discussion

The selected set of stars is to large extent repeated for several orbits until the stars are out of the field-of-view. Occultations of the same star at successive orbits are made at the same latitude band but with varying longitude (about 15/day). In Fig. 4 the latitude coverage of the night time occultations during 2003 are shown. The individual stars can typically be followed for several months in a row.

2.2.2 Geographical distribution of GOMOS measurements

The GOMOS measurements cover the whole globe from pole to pole. This can be seen in Fig. 5 where the geographical distribution of the GOMOS night time measurements from summer 2002 to autumn 2009 are shown. We see that quite a good global coverage can be obtained using 10 deg latitude bands. In particular, the unique measurements of GOMOS during polar night have been utilized extensively e.g., in studies of long term effects of solar proton events during polar night (Seppälä et al., 2007; Verronen et al., 2005) and in studying the effect of intense warming and air descent Hauchecorne et al. (2007).

Depending on the season, there is some variation in the distribution of the measurements as the stars are not distributed evenly in the sky (see Fig. 5). In addition, the night time measurements do not cover the summer pole. The calibration measurements that are performed at each orbit close to the equator cause some reduction in the number of occultations there.

The yearly variations in the measurement distribution are caused by technical problems in the instrument. In May 2003 there was a technical anomaly and the number of measurements was low during May and June in 2003. After another technical anomaly that took place in January 2005 the viewing angle was slightly reduced and the number of (night-time) profiles went down from about 200 to 150 profiles per day. In 2009 the number of occultations has been clearly less than in the previous years and this is again due to technical anomalies that caused the the occultations stop already at high altitudes. In December 2009 the situation improved and since then the performance has been almost normal (not shown in figure).

In principle, GOMOS measures each year the same stars at the same latitude regions which is very useful when making a time series analysis based on the data. Some changes have, however, taken place during the mission due to the reduced viewing angle. Moreover, it is important to keep in mind that there are differences in the overall global coverage and some latitude bands are covered more densely that the others.

2.2.3 Altitude range

The GOMOS instrument is equipped with the star tracker operating at 625–950 nm, which follows the star by keeping the image of the star in the centre of the slit. The technique has turned out to work reliably (except the last technical anomaly in 2009) and the stars can typically be tracked from the top of the atmosphere (120–150 km) down to 5–20 km tangent altitude. It seems that when no clouds are present, stars can be followed as low as 5 km altitude (especially bright stars). The presence of clouds in the field-of-view leads to loosing the signal. Other factors affecting the lowest altitude are stellar brightness (the brighter the star, the lower the tangent altitude) and regular refraction (the star image can fall outside the field-of-view due to refraction). Figure 6 shows the lowest measurement altitude for 30 brightest stars (with visual magnitudes < 1.6). This distribution is in very good general agreement with the maps of the cloud top height (e.g., http://isccp.giss.nasa.gov/index.html), thus indicating that the main reason for terminating the occultations of bright stars is the presence of clouds. In tropics, the lowest altitude is 15–18 km because of frequent presence of high clouds (cirrus and convective clouds). Above South Pole the measurements are also often terminated at 15–18 km, most probably because of frequent occurrence of polar stratospheric clouds (note that polar regions are not covered by GOMOS in summer). The lowest altitude in occultations of bright stars can potentially provide valuable information about cloud top height.

3 Error propagation through GOMOS retrieval

The random error plays an important role in the GOMOS total error budget, unlike what is the case in several other remote sensing instruments which are dominated by systematic errors. The random errors in GOMOS data are mainly due to the propagation
5 of the measurement noise and the imperfect scintillation correction. First we discuss how the measurement noise is propagated through the GOMOS retrieval steps. The GOMOS retrieval procedure is described in details in Kyrölä et al. (2010) and we will use here the same notation as much as possible.

The GOMOS data retrieval is based on describing the measurement and the quan-
10 tities to be retrieved as random variables. By error propagation we mean how the measurement noise and possible modelling errors impact the uncertainty of the retrieved quantities. In the GOMOS retrieval procedure we apply the Bayesian theorem and describe the solution as *a posteriori distribution* which is in practice approximated with Gaussian distribution whose mode and covariance are computed. The covariance
15 matrix describes the uncertainty of the retrieved quantities.

3.1 Error propagation through spectral inversion

The GOMOS retrieval problem is solved in two steps which are called *spectral inversion* and *vertical inversion*. In spectral inversion horizontally integrated column densities of O_3, NO_2, NO_3 and aerosols are simultaneously fitted to the transmission data T_{ext}^{obs}
20 (which is corrected for refractive effects, see Eq. (32) in Kyrölä et al., 2010). Measurements at successive tangent altitudes are treated separately. Assuming that the noise in the transmission is Gaussian, the problem of finding maximum a posteriori point is equal with finding the solution that minimizes the sum of squared residuals term:

$$SSR = (T_{ext} - T_{ext}^{obs})C^{-1}(T_{ext} - T_{ext}^{obs})^T \qquad (1)$$

25 where T_{ext} refers to the modelled transmission which depends on the horizontally integrated densities $(\overline{N})$ of the gases that are fitted according to Beer law, see Eq. (42) in

Kyrölä et al. (2010). The covariance matrix C includes both measurement and modelling errors. In the present GOMOS processing (IPF Version 5) the modelling error is ignored, but in the updated version (IPF Version 6) this is also taken into account (see Sect. 4.1). The inverse problem is non-linear and it is solved iteratively by applying
5 Levenberg-Marquardt algorithm (Press et al., 1992). The algorithm assumes that the posterior distribution is roughly Gaussian close to the point that minimizes the sum of squared residuals, so that the posterior distribution of the horizontal column densities can characterized with the estimate and the covariance matrix $C_{\overline{N}}$. The posterior covariance matrix is also returned by the Levenberg-Marquardt algorithm. The diagonal
10 elements of the covariance matrix characterize the variance of the error estimates of the horizontal column densities.

Instead of using a fast iterative algorithm one can apply more time consuming Monte Carlo methods to compute the real posterior distribution to analyse the validity of the assumption of Gaussian posterior distribution. The Markov chain Monte Carlo (MCMC)
15 technique has been successfully applied to the GOMOS spectral inversion (Tamminen and Kyrölä, 2001; Tamminen, 2004). It has been shown that Gaussian posterior distribution is a good approximation in the GOMOS spectral inversion (Tamminen, 2004).

3.1.1 Correlated errors after spectral inversion

The absorption cross sections of gases and aerosols are not independent and there-
20 fore the retrieval errors of these constituents can also be correlated. The amount of correlation changes depending on the altitude due to the changing effective wavelength region. The off-diagonal values of the posterior covariance matrix $C_{\overline{N}}$ describe the correlations in the errors. In Fig 7 we give an example of the the correlation coefficients ($R_{\overline{N}}(i,j) = C_{\overline{N}}(i,j) / \sqrt{(C_{\overline{N}}(i,i)C_{\overline{N}}(j,j))}$) between the errors in O_3 and the other
25 retrieved parameters (NO_2, NO_3, and three aerosol parameters) after the spectral inversion. In the figure, the correlation coefficients are plotted for all retrieval altitudes. We note that, in this case, the error estimates of the horizontally integrated column O_3 are mainly correlated with the aerosol errors and this has largest impact below about

25 km. Some positive correlation with O_3 and NO_2 column errors can also be seen, but that is generally below 0.4. The maximum correlation ($\sim$0.5) seems to be around 20–40 km depending on the stellar type and the atmospheric composition. The correlation between O_3 and NO_3 is negligible. The correlation structure varies somewhat depending on the stellar characteristics and the example given in Fig. 7 corresponds to a hot star.

In principle, the correlation in errors should be taken into account when analysing, e.g., the correlations of gases. However, this is typically not done, and in GOMOS case this information is not available for profiles but only for horizontally integrated column densities after the spectral inversion. A simplified simulation study was performed in order to get an idea how much the correlated errors impact if we want to estimate the correlation of the gases (e.g., O_3 and NO_2). The study showed that the estimated correlation of the gases was only very slightly biased when the correlation in their errors was not taken into account. However, the accuracy of the estimated correlation of the gases was more influenced. Based on this exercise we can conclude that when using GOMOS data to study correlation between O_3 and NO_2 or aerosols the significance of the correlation may be either overestimated or underestimated. If the correlation we found is negative/positive and the errors are also correlated negatively/positively then the significance of the correlation is underestimated and if the errors are correlated differently, positively/negatively, then the significance of the correlation is overestimated.

3.1.2 Random error propagation through vertical inversion

In the vertical inversion the horizontally integrated column densities are transformed to local densities using information about the ray path of the measurement. Each constituent is treated separately and the correlations between the errors of the horizontal column densities are not taken into account, see Kyrölä et al. (2010) for description.

The vertical inversion is linear so the error propagation can be directly estimated using standard techniques. Let us assume that $C_{\overline{N}}$ denotes the estimated error covariance (which is diagonal matrix) of horizontal column density profile of one constituent

after the spectral inversion. Now the covariance matrix of the retrieved profile is simply

$$C_\rho = LC_{\overline{N}}L^T, \tag{2}$$

where L is the retrieval matrix so that $\rho = L\overline{N}$ (corresponding to Eq. (49) in Kyrölä et al. (2010)). The diagonal elements of of the posterior covariance matrix C_ρ describe the

5 variance of the estimated local density values whereas the off-diagonal elements of the covariance matrix C_ρ characterize the correlation between the retrieved densities at successive layers. In GOMOS data products six most significant off-diagonal elements are reported. After applying the Tikhonov regularization the errors of the nearby layers are somewhat correlated, see Fig. 8 where the correlation coefficients for the

10 ozone retrieval ($R_\rho(i,j) = C_\rho(i,j)/\sqrt{(C_\rho(i,i)C_\rho(j,j))}$) are plotted for five selected altitudes. We see that, above 35 km where the Tikhonov regularization is stronger, also the correlation in the errors is larger, and involves about 3 layers above and below the retrieval height. Below 30 km only errors from 2 layers below and above the retrieval altitude are slightly correlated. In oblique occultations there is a larger correlation be-

15 tween the errors at neighbouring layers because the regularization is stronger than in the vertical occultations.

4 Modelling errors

In the GOMOS retrieval the faint signal is compensated by using a wide spectral window for the data processing. The advantage is clear – we maximize the use of the

20 data, but, as a drawback, the consistency in the modelling of the wide wavelength band becomes much more important. In the GOMOS spectral inversion residuals (i.e., measured transmission spectra minus modelled ones) we see some structures which are mainly due to imperfect scintillation correction. They are considered as the largest modelling error in the GOMOS retrieval. The imperfect modelling of the aerosol con-

25 tribution is an important source of modelling error especially at low altitudes. Other

sources of modelling error are uncertainties in the absorption cross sections and temperature. Relatively negligible impact is seen due to uncertainty of neutral density profile, ray path computation and potentially missing constituents.

4.1 Scintillation – dilution correction

When the stellar light traverses through the atmosphere, it is affected also by the refractive effects, dilution and scintillation, which need to be taken into account in the retrieval. The approach taken in the GOMOS data processing is to remove these effects before performing the inversion (see Kyrölä et al., 2010 for general description of the algorithms).

The dilution term is approximated using ECMWF air density. As the refraction can be accurately computed, the error caused by this assumption is negligible in the retrieved profiles (Sofieva et al., 2006).

In the GOMOS retrievals, the perturbations in the stellar flux caused by scintillations are corrected by using additional scintillation measurements by the fast photometer operating in low-absorption wavelength region (Dalaudier et al., 2001; Sofieva et al., 2009). The quality of the scintillation correction and its limitations are discussed in Sofieva et al. (2009) where it was shown that the applied scintillation correction removes significant part of the perturbations in the recorded stellar flux caused by scintillations, but it is not able to remove scintillations generated by the isotropic turbulence. The remaining perturbations, due to the incomplete scintillation correction, are not negligible: in oblique occultations of bright stars, they can be comparable or even exceed the instrumental noise by a factor of 2–3 at the altitude 20–45 km (Sofieva et al., 2009) (Fig. 9). This causes about 0.5–1.5% additional error in the ozone retrievals at the altitude range of 20–45 km (Sofieva et al., 2009).

The modelling error caused by the imperfect scintillation correction can be taken into account in the spectral inversion by introducing a wavelength correlated modelling error contribution to the retrieval. The parametrisation of the scintillation correction errors is presented in Sofieva et al. (2009). In the proposed parametrization, which is based

on statistical analyses of GOMOS residuals and the theory of isotropic scintillations, the scintillation correction error is assumed to be a Gaussian random variable with zero mean and a non-diagonal covariance matrix (Sofieva et al., 2009). When the scintillation correction errors are taken into account, the normalized χ^2 values which reflect the agreement between the measurement and modelling become close to the optimal value 1. This improvement ensures that the estimated accuracy of the retrieved profiles is closer to the reality after including the modelling error component to the retrieval. In the present operational GOMOS Level 2 algorithm (IPF Version 5) this is not included, but it will be implemented in the new IPF Version 6 in spring 2010.

The incomplete scintillation correction is the main source of GOMOS modelling errors in the stratosphere (at altitudes 20–45 km). However, this modelling error is not systematic but random in nature. By averaging measurements on successive layers or requiring smoothness of the retrieved profile (as is done in GOMOS vertical inversion) the impact of this modelling error reduces.

4.2 Uncertainty in aerosol modelling

In the GOMOS spectral inversion absolute cross sections are used and the aerosols are also inverted simultaneously with the trace gases. The aerosol cross sections depend on the aerosol size distribution and composition which are unknown. A practical approach is to use a simplified wavelength dependent model for the aerosol cross sections. In the present algorithm, aerosol cross sections are assumed to depend on the wavelength, λ, according to a second order polynomial (see Kyrölä et al., 2010 for details of the algorithm). Three parameters are fitted. The choice of using second order polynomial is somewhat arbitrary and first or third order polynomials could also be considered.

A sensitivity study was made in order to quantify the modelling error caused by using a simplified aerosol model. This was done by comparing retrieval results using 7 different aerosol models, namely constant (A-1), first (A-2), second (A-3) and third order (A-4) polynomial in λ and first (A-5), second (A-6) and third order polynomial (A-7) in

$\frac{1}{\lambda}$. Aerosol model A-3 corresponds to the one that is used in the operational GOMOS data processing IPF (both Versions 5 and 6). As a test case we used took than 1000 occultations and compared the median values in this set, see Fig. 9. These results are obtained using the presently available GOMOS Version 5 processing. We note that the (physically most unrealistic) model A-1 gives quite different results than the others. By comparing the impact of the other models we can conclude the following. The aerosol model selection has its largest impact at low altitudes below 20 km. For ozone the sensitivity is of the order of 20% below 20 km and 1–5% between 20–25 km. Above 25 km the uncertainty in the aerosol modelling does not have much impact to ozone retrieval. For NO_2 the impact is typically around 10% between 15–20 km. Above 20 km the impact is small, less than 5%. For NO_3 the impact can be as large as 100% around 15–20 km, but above 25 km, which is the lowest reasonable altitude for NO_3, it does not affect the results significantly. The impact in aerosol extinction is below 10% up to 35 km and larger above.

In a recent publication, a technique for selecting the best aerosol model in the GOMOS spectral inversion is developed using Markov chain Monte Carlo technique (Laine and Tamminen, 2008). It is shown that the model selection can be implemented simultaneously with the parameter estimation to the spectral inversion. More work is, however, needed to show the quantitative advantage in practice.

4.3 Uncertainty of cross sections and atmospheric temperature

The retrieval of the atmospheric constituents from the GOMOS measurements is based on assuming a good knowledge of the cross sections of the retrieved gases O_3, NO_2 and NO_3. See Kyrölä et al. (2010) for more details of the cross sections that are used in GOMOS retrievals. The errors in the cross sections are, unfortunately, not well known. Some studies, assuming independent Gaussian distributed uncertainty have been performed, but the validity of these estimates is, however, limited, since the uncertainty is not realistically modelled. By comparing several sets of laboratory measured O_3 cross sections, it is obvious that these measurements include also uncertainties both in the

absolute values and also in their temperature dependence, and the uncertainties are not independent (see e.g., Burrows et al., 1999). When the nature of the uncertainty is not known, it is also difficult to take into account in the inverse problem. By making a sensitivity study and using different sets of ozone cross sections in GOMOS spectral inversion we observe a difference of the order of 1–1.5% in ozone retrieval.

The absorption cross sections of O_3, NO_2 and NO_3 depend also on the temperature and, therefore, some error is also caused by the uncertainty in the atmospheric temperature. In some sense, part of the systematic bias in the cross sections could, actually, be modelled as the uncertainty in the temperature. Unlike in several other instruments, in the operational GOMOS retrieval the atmospheric temperature is not fitted but assumed to be known. For that ECMWF temperature below 50 km is used and MSIS90 temperature above 50 km. If moderate Gaussian uncertainty (with zero mean and 2 K standard deviation) in the temperature information is taken into account the error in O_3 retrieval increases slightly ($< 0.5\%$) at 30–60 km altitude range (Tamminen, 2004). At this altitude the retrieval is based on Huggins band where the cross sections are known to be strongly temperature dependent. The impact is less significant with NO_2 and NO_3 retrievals which are more dominated by the random measurement noise.

Further work is still needed to understand the nature of the uncertanties in the cross sections and to properly estimate the impact in the GOMOS products. This work will be contiued as a part of the IGACO-O3/UV activity, initiated by IO3C (International Ozone Commision) and WMO-GAW, on the evaluation of the absoption cross sections of ozone (ACSO, see http://igaco-o3.fmi.fi/ACSO/). This activity, which involves several ground based and satellite instruments using the Huggins band, will be finalized by 2011.

4.4 Uncertainty of neutral density profile

In earlier versions of the GOMOS data processing also the neutral density was inverted simultaneously with O_3, NO_2, NO_3 and aerosols. Due to the similar nature of Rayleigh scattering cross sections and aerosol scattering cross sections these two quantities

are strongly correlated. In order to improve the aerosol retrieval it was decided to fix the the neutral density concentration using ECMWF analysis values below 50 km and to use MSIS90 model values above. Assuming, that the uncertainty of ECMWF neutral density is around 2% we observe negligible (< 1%) impact for O_3, NO_2 and

5 NO_3 retrievals. However, in aerosol retrieval the impact is larger. Around 22–40 km the impact is generally around 5–10% (with maximum impact around 27 km 15%). Below 22 km the impact is less significant being smaller than 5%.

4.4.1 Missing constituents

The wavelength band 248–690 nm that is used for retrieval of O_3, aerosols, NO_2 and
10 NO_3 contains also absorption by OClO, BrO and Na. However, in individual retrievals their impact is so small that the error caused by not including them in the modelling is negligible. Only by averaging several hundreds of measurements the signatures of, e.g., Na can be seen (Fussen et al., 2004). The wavelengths that include O_2 signature at 627–630 nm are excluded from the inversion.

15 ## 4.5 Uncertainty in ray tracing and measurement position

One of the advantages of the stellar occultation technique is that the measurement target is a point source whose position is well known. Therefore, the uncertainty in the ray path and its tangent altitude is only due to the uncertainty in the satellite position and the ray path calculation. The position of the Envisat satellite is also well known so
20 the impact of this uncertainty is rather small, of the order of 30 m (Bertaux et al., 2010). The ray path calculation is done using the ECMWF neutral density analysis data and it causes at maximum about 15 m error in the tangent altitude for ray paths at 10 km altitude range, above that the impact is smaller and <5 m for rays above 20 km altitude (Sofieva et al., 2006).

25 In conclusion, the uncertainty in the GOMOS measurement ray path cause only negligible uncertainty to atmospheric profiles. This is also confirmed by several validation

studies where no altitude shift has been found (see e.g., Meijer et al., 2004; Bertaux et al., 2010).

5 Vertical resolution

Due to the stellar occultation measurement principle and measurement geometry the vertical resolution of GOMOS is very good. The sampling resolution of GOMOS is between 0.5–1.7 km. When the occultation takes place in the orbital plane the sampling resolution is lowest (1.7 km) and when the occultation is more on side the sampling resolution becomes denser. Due to the refraction the sampling resolution becomes also denser below 40 km and reaches its maximum at the lowest altitudes.

The resolution of retrieved profiles is a combination of the measurement itself and the retrieval technique. A commonly used way of analysing the resolution of the retrieved profile (and the correlations between the densities of successive layers) is to plot the so called averaging kernels. Averaging kernels are defined as the dependence on the retrieved profile $\widehat{\rho}$ on the true profile ρ (see e.g. Rodgers, 2000)

$$A = \frac{\partial \widehat{\rho}}{\partial \rho}. \tag{3}$$

A typically used measure for the resolution is so called Backus-Gilbert spread which is defined as the *spread* of the averaging kernels around the level z_0 defined as

$$s(z_0) = 12 \frac{\int A^2(z)(z - z_0)^2 dz}{\left(\int A(z) dz \right)^2} \tag{4}$$

(see e.g., Rodgers, 2000).

In GOMOS vertical inversion Tikhonov type of smoothing is applied (Tamminen et al., 2004; Sofieva et al., 2004; Kyrölä et al., 2010). Since the sampling resolution changes from occultation to occultation it was decided that instead of finding the optimal amount

of smoothing to each occultation separately, the amount of smoothing is defined so that the retrieved profiles have the same resolution. This choice makes it easier for the end users to use GOMOS profiles since there is no need to use different averaging kernels for each occultation to interpret the measurements. In addition, more

5 smoothing is automatically applied by this technique to oblique occultations, which is advantageous since they suffer more from scintillations. The applied target resolutions of different constituents are given in Table 2. The choice of the target resolution for O_3 was partly based on the case study of the O_3 profile smoothness analysed by Sofieva et al. (2004). The impact of the GOMOS vertical inversion is demonstrated in Fig. 10 by

10 showing the resolution of the O_3 profile for three occultations with different measurement geometries. In the figure the Backus-Gilbert spread is shown first without and then with applying the Tikhonov-regularization and the *target resolution* technique. We observe that, regardless of the sampling resolution of the occultations, the retrieved profiles have all the same resolution which is around 2 km at lower stratosphere and

15 around 3 km in the upper stratosphere and mesosphere.

In Fig. 11 typical examples of GOMOS averaging kernels for O_3, NO_2 and NO_3 are shown. The GOMOS averaging kernels are very sharp and peak clearly at the retrieval altitude showing the excellent vertical resolution that can be obtained with the stellar occultation technique. The stronger smoothing applied for NO_2 and NO_3 retrievals can

20 be seen as the wider averaging kernels compared to O_3 averaging kernels.

As typically done in retrievals of limb instruments, spherically symmetric atmosphere around the tangent point of each occultation is locally assumed also in the GOMOS retrieval. The Envisat/GOMOS measurement geometry is such that the length of the ray path inside the atmospheric below 100 km with 15 km tangent altitude is about 2100 km.

25 The impact of the spherical symmetry assumption depends on the atmospheric conditions and is naturally largest around poles where strong atmospheric gradients are found during polar vortex periods. When analysing the ozone profiles from limb viewing instruments it is important to keep this representation issue in mind.

6 GOMOS error estimates

6.1 GOMOS random error estimates of O_3, NO_2, NO_3 and aerosols

The main contributor in GOMOS error budget is the random measurement noise. In Fig. 12 examples of the random error estimates of O_3, NO_2, NO_3 and aerosols are shown for representative star types. These error estimates, also known as the precision, characterize the random error component in GOMOS retrieval (both spectral and vertical inversion) that consist of the propagation of the measurement noise (as discussed in Sect. 3) and the random modelling error caused by incorrect scintillation correction. For each of the constituents we show the error estimates of both oblique (dashed lines) and vertical measurement geometry (solid lines). Note, that the examples correspond to particular atmospheric conditions, so slight inconsistency can be seen in some of the curves since it was decided to present the relative values. In general, the error estimates are smallest in the case of bright stars (column on left) and largest with dim stars (column on right).

The random error of O_3 varies depending on the altitude range and the stellar type. With hot and medium temperature stars that are also bright or medium brightness the ozone profiles can be measured up to 100 km altitude with the precision of less than 8%. At the O_3 minimum, around 80 km, the precision is the worst. The precision is smallest around 40–60 km where it is typically 0.5–2%. Above 40 km it is not recommended to use the cool stars because they suffer from low signal-to-noise ratio. Below 40 km the O_3 can be measured with also the cool and the dim stars. The precision between 20–40 km is around 1–3% and below 20 km it is degrading to 10% at 15 km. Below 15 km the precision degrades strongly and individual occultations do not carry much information.

The precision of the NO_2 retrieval is not as strongly dependent on the stellar type as the O_3 retrieval is. With reasonably bright stars NO_2 can be measured at 20–50 km altitude range with 10–20% precision. In the case of high NO_2 concentration, e.g., after a strong solar proton event, NO_2 can be measured up to 65 km altitude (not shown

[ACPD](#)

10, 6755–6796, 2010

GOMOS data characterization

J. Tamminen et.al

Title Page

Abstract | Introduction

Conclusions | References

Tables | Figures

◀ | ▶|

◀ | ▶

Back | Close

Full Screen / Esc

Printer-friendly Version

Interactive Discussion

here).

The NO_3 can be measured with 25–45 km altitude range with the precision of 20–40% with the bright and the medium brightness stars. Slightly better results are obtained with the cool stars.

The aerosols can be measured from 15 km up to 30 km with about 5–10% precision. Below 15 km the precisions degrades to 30%. The stellar temperature does not have a significant impact on the aerosol results.

The impact of the scintillation is related to the occultation geometry. In the Fig. 12 the error estimates for both the oblique and vertical occultations are given. It can be observed that, despite that the scintillation effect is largest at the oblique occultations, this does not show up so strongly in the results. For O_3 we observe slightly degrading (about 1–2%) error estimates at 20–40 km altitude range. In the oblique occultations the vertical sampling becomes denser and when the smoothing is applied using the *target* resolution there is more measurements that are effectively used in the smoothing, compensating the noisy measurements more in the oblique geometry. At the high altitudes, e.g., around the second O_3 maximum, the precision is best in the case of oblique occultations.

The error estimates shown in Fig. 12 correspond to the error estimate values reported in the GOMOS data products together with the profile data in the upcoming IPF Version 6. In IPF Version 5 the reported error estimates include measurement noise and an (overestimated) ad-hoc estimate for the scintillation contribution.

6.2 Instrument aging

As the instrument ages the amount of dark charge on the GOMOS CCD detectors increases. This impacts directly the signal-to-noise ratio of the measurements and can also be seen as a slight decrease in the data quality. By analysing the data quality of occultations close to equator where the changes in the gas concentrations are small we can see how the aging impacts the error estimates. In Fig. 13 the yearly changes (median over each year) of the O_3 error estimates at 50 km are seen. The altitude

region was selected to be above the altitude range affected by the scintillations and the occultations were selected to be close the equator where the natural variability is considered to be smallest. The aging seems to have the largest impact on stars with weaker signal-to-noise ratio (star 124). In the examples shown in Fig. 13 we see that the error estimates get almost twice as large, from 1.5% to 3% in 7 years (2002–2008) whereas the change in stars with higher signal-to-noise ratio (stars 9 and 29) is small, less than 0.5% in 5 years (2003–2007). These results were obtained using the GOMOS processor IPF Version 5 but similar values are expected in Version 6 as well.

7   Summary

The stellar occultation instrument GOMOS, on-board the Envisat satellite, was launched in 2002. Since then, it has provided global measurements of trace gas and aerosol profiles with high vertical resolution of 2–4 km. The altitude range of GOMOS extends typically from tropopause to 100 km. We have here discussed the data characterization and error estimation of O_3, NO_2, NO_3 and aerosol profiles of GOMOS night time occultations.

The GOMOS data characteristics together with the random and the systematic errors are summarized in Table 3. The main sources of the GOMOS errors are due to random effects: measurement noise and scintillations. The largest part of the systematic error is due to imperfect aerosol modelling which impacts mainly the O_3 and aerosol retrievals. The valid altitude range for the O_3 measurements is roughly 15–100 km, for NO_2 20–50 km with the exception that when there is a high NO_2 load in the upper atmosphere, e.g., due to solar proton event, the valid altitude range extends up to 65 km. NO_3 can be measured at 25–45 km and aerosols 10–40 km. In the GOMOS products also data at the other altitudes, outside the range considered to be valid, are given. If this data are used, it is recommended that, special attention to the data quality is taken. The error estimates that are reported together with the GOMOS profiles do not include the systematic errors.

The GOMOS Level 1b and Level 2 data are freely avail- able via ESA website (http://http://eopi.esa.int/esa/esa?cmd=submission\&aoname=cat1) but registration is required. Instructions how to register and get GOMOS off-line data and GOMOS near real time data can be found at http://envisat.esa.int/handbooks/gomos/CNTR3.htm A comprehensive documentation for the GOMOS instrument including the data disclaimer can be found at http://envisat.esa.int/handbooks/gomos/. The GOMOS Algorithm theorem basis document (ATBD) can be found at http://envisat.esa.int/instruments/gomos/atbd/.

References

Bertaux, J. L., Hauchecorne, A., Dalaudier, F., Cot, C., Kyrölä, E., Fussen, D., Tamminen, J., Leppelmeier, G. W., Sofieva, V., Hassinen, S., d'Andon, O. F., Barrot, G., Mangin, A., Théodore, B., Guirlet, M., Korablev, O., Snoeij, P., Koopman, R., and Fraisse, R.: First results on GOMOS/Envisat, Adv. Space Res., 33, 1029–1035, 2004. 6757

Bertaux, J.-L., E., K., Fussen, D., Hauchecorne, A., Dalaudier, F., Sofieva, V., Tamminen, J., Vanhellemont, F., Fanton d'Andon, O., Barrot, G., Mangin, A., Blanot, L., Lebrun, J., Fehr, T., Saavedra, L., and Fraisse, R.: Global Ozone Monitoring by Occultation OF stars: an overview of GOMOS measurements on ENVISAT, Atmos Chem. Phys. Discuss., in review, 2010. 6757, 6758, 6771, 6772

Burrows, J. P., Richter, A., Dehn, A., Deters, B., s. Himmelmann, Voigt, S., and Orphal, J.: Atmospheric remote-sensing reference data from GOME – 2. temperature-dependent absorption cross sections of O_3 in the 231–794 nm range, J. Quant. Spectrosc. Radiat. Transfer, 61, 509–517, 1999. 6770

Dalaudier, F., Kan, V., and Gurvich, A. S.: Chromatic refraction with global ozone monitoring by occultation of stars. I. Description and scintillation correction, Appl. Opt., 40, 866–877, 2001. 6767

GOMOS data characterization

J. Tamminen et.al

Fussen, D., Vanhellemont, F., Bingen, C., Kyrölä, E., Tamminen, J., Sofieva, V., Hassinen, S., Seppälä, A., Verronen, P., Bertaux, J.-L., Hauchecorne, A., Dalaudier, F., Renard, J.-B., Fraisse, R., Fanton d'Andon, O., Barrot, G., Mangin, A., Théodore, B., Guirlet, M., Koopman, R., Snoeij, P., and Saavedra, L.: Global measurement of the mesospheric sodium layer by the star occultation instrument GOMOS, Geophys. Res. Lett., 31, L24110, doi:10.1029/2004GL021618, 2004. 6771

Hauchecorne, A., Bertaux, J.-L., Dalaudier, F., Russell, J. M., Mlynczak, M. G., Kyrölä, E., and Fussen, D.: Large increase of NO_2 in the north polar mesosphere in January-February 2004: Evidence of a dynamical origin from GOMOS/ENVISAT and SABER/TIMED data, Geophys. Res. Lett., 34, 3810, doi:10.1029/2006GL027628, 2007. 6761

Hays, R. G. and Roble, P. B.: Stellar spectra and atmospheric composition, J. Atmos. Sci., 25, 1141–1153, 1968. 6757

Kyrölä, E. and Tamminen, J.: GOMOS mission planning, in: ESAMS99, European Symposium on Atmospheric Measurements from Space, WPP-161, 101–110, ESA, Noordwijk, 1999. 6760

Kyrölä, E., Tamminen, J., Leppelmeier, G. W., Sofieva, V., Hassinen, S., Bertaux, J.-L., Hauchecorne, A., Dalaudier, F., Cot, C., Korablev, O., d'Andon, O. F., Barrot, G., Mangin, A., Theodore, B., Guirlet, M., Etanchaud, F., Snoeij, P., Koopman, R., Saavedra, L., Fraisse, R., Fussen, D., and Vanhellemont, F.: GOMOS on Envisat: An overview, Adv. Space Res., 33, 1020–1028, 2004. 6757

Kyrölä, E., Tamminen, J., Sofieva, V., Bertaux, J.-L., Hauchecorne, A., Dalaudier, F., Blanot, L., Fussen, D., Vanhellemont, F., d'Andon, O. F., Barrot, G., Mangin, A., Guirlet, M., Fehr, T., de Miguel, L. S., and Fraisse, R.: Retrieval of atmospheric parameters from GOMOS data, Atmos. Chem. Phys. Discuss. in review, 2010. 6758, 6763, 6764, 6765, 6766, 6767, 6768, 6769, 6772

Laine, M. and Tamminen, J.: Aerosol model selection and uncertainty modelling by adaptive MCMC technique, Atmos. Chem. Phys., 8, 7697–7707, 2008, http://www.atmos-chem-phys.net/8/7697/2008/. 6769

Meijer, Y. J., Swart, D. P. J., Allaart, M., Andersen, S. B., Bodeker, G., Boyd, Braathena, G., Calisesia, Y., Claude, H., Dorokhov, V., von der Gathen, P., Gil, M., Godin-Beekmann, S., Goutail, F., Hansen, G., Karpetchko, A., Keckhut, P., Kelder, H. M., Koelemeijer, R., Kois, B., Koopman, R. M., Lambert, J.-C., Leblanc, T., McDermid, I. S., Pal, S., Kopp, G., Schets, H., Stubi, R., Suortti, T., Visconti, G., , and Yela, M.: Pole-to-pole validation of ENVISAT/GOMOS

GOMOS data characterization

J. Tamminen et.al

ozone profiles using data from ground-based and balloon-sonde measurements, J. Geophys. Res., 109, D23305, doi:10.1029/2004JD004834, 2004. 6772

Press, W. H., Teukolsky, S. A., Vetterling, W. T., and Flannery, B. P.: Numerical Recipes in FORTRAN, The Art of Scientific Computing, Clarendon Press, Oxford, 1992. 6764

Rodgers, C. D.: Inverse Methods for Atmospheric sounding: Theory and Practice, World Scientific, Singapore, 2000. 6758, 6772

Seppälä, A., Verronen, P. T., Clilverd, M. A., Randall, C. E., Tamminen, J., Sofieva, V. F., Backman, L., and Kyrölä, E.: Arctic and Antarctic polar winter NO_x and energetic particle precipitation in 2002–2006, Geophys. Res. Lett., 34, L12810, doi:10.1029/2007GL029733, 2007. 6761

Sofieva, V., Tamminen, J., and Kyrölä, E.: Modeling errors of GOMOS measurements: A sensitivity study, in: Atmosphere and Climate, Studies by Occultation Methods, edited by: Foelsche, U., Kirchengast, G., and Steiner, A., 67–78, Springer, 2006. 6767, 6771

Sofieva, V. F., Tamminen, J., Haario, H., Kyrl, E., and Lehtinen, M.: Ozone profile smoothness as a priori information in the inversion of limb measurements, Ann. Geophys., 22, 3411–3420, 2004,
http://www.ann-geophys.net/22/3411/2004/. 6772, 6773

Sofieva, V. F., Kan, V., Dalaudier, F., Kyrölä, E., Tamminen, J., Bertaux, J.-L., Hauchecorne, A., Fussen, D., and Vanhellemont, F.: Influence of scintillation on quality of ozone monitoring by GOMOS, Atmos. Chem. Phys., 9, 9197–9207, 2009,
http://www.atmos-chem-phys.net/9/9197/2009/. 6767, 6768

Tamminen, J.: Validation of nonlinear inverse algorithms with Markov chain Monte Carlo method, J. Geophys. Res., 109, D19303, doi:10.1029/2004JD004927, 2004. 6764, 6770

Tamminen, J. and Kyrölä, E.: Bayesian solution for nonlinear and non-Gaussian inverse problems by Markov chain Monte Carlo method, J. Geophys. Res., 106, 14 377–14 390, 2001. 6764

Tamminen, J., Kyrölä, E., and Sofieva, V.: Does prior information improve measurements?, in: Occultations for Probing Atmosphere and Climate - Science from the OPAC-1 Workshop, edited by: Kirchengast, G., Foelsche, U., and Steiner, A., 87–98, Springer Verlag, 2004. 6772

Verronen, P. T., Seppälä, A., Clilverd, M. A., Rodger, C. J., Kyrölä, E., Enell, C.-F., Ulich, T., and Turunen, E.: Diurnal variation of ozone depletion during the October–November 2003 solar proton events, J. Geophys. Res., 110, A09S32, doi:10.1029/2004JA010932, 2005. 6761

Vervack, R. J., Yee, J., DeMajistre, R., and Swartz, W. H.: Intercomparison of MSX/UVISI-derived ozone and temperature profiles with ground-based, SAGE II, HALOE, and POAM III data, J. Geophys. Res., 108, 2–1, 2003. 6757

Yee, J.-H., Jr., R. J. V., Demajistre, R., Morgan, F., Carbary, J. F., Romick, G. J., Morrison, D., Lloyd, S. A., DeCola, P. L., Paxton, L. J., Anderson, D. E., Kumar, C. K., and Meng, C.-I.: Atmospheric remote sensing using a combined extinctive and refractive stellar occultation technique, 1. overview and proof-of-concept observations, J. Geophys. Res., 107, 101029, doi:10.1029/2001JD000794, 2002. 6757

Table 1. Occultation statistics during time period 2002–2008 divided by different stellar classes depending on brightness and approximated surface temperature.

	Bright $M_v<0.8$	Medium M_v:0.8–2	Dim $M_v>2$	Tot
Cool, $T \leq 6000$ K	3%	7%	22%	32%
T:6000–10 000 K	5%	4%	11%	19%
Hot, $T \geq 10\,000$ K	11%	20%	18%	49%
Tot	18%	31%	51%	100%

Table 2. Resolution of the GOMOS profile products.

Gas	≤30 km	30–40 km	≥40 km
O_3	2 km	2–3 km	3 km
NO_2, NO_3	4 km	4 km	4 km
aerosols	4 km	4 km	4 km

Table 3. GOMOS data characteristics and error contributions due to systematic and random errors. The values correspond to the night time measurements. For NO_2 the higher altitude limit corresponds to case with high NO_2 concentration. (*) The impact of the systematic errors due to the uncertainty in cross sections for NO_2 and NO_3 is only rough estimate.

Data characteristics	O_3	NO_2	NO_3	Aerosol extinction
Altitude range range	15–100 km	20–50 (65) km	25–50 km	10–40 km
Resolution	2 km stratosphere 3 km mesosphere	4 km	4 km	4 km
Random errors: Measurement noise and scintillations	10% around 15 km 0.5–4% stratosphere 2–10% mesosphere	10–20%	20–40%	30% around 10 km 2–10% at 15–25 km 10–50% 25–40 km
		slightly increasing with time		
Systematic errors: Aerosol model selection	~20% below 20 km 1–5% at 20–25 km <1% above 25 km	~10% at 15–20 km 0–5% at 20–25 km negligible elsewhere	negligible above 25 km	<10% below 35 km 10–50% at 35–40 km
Temperature uncertainty	<0.5% at 30–60 km negligible elsewhere	negligible	negligible	–
Uncertainty in cross sections	~1%	few per-cents (*)	few per-cents (*)	–
Uncertainty in neutral density	<1% below 20 km negligible elsewhere	negligible	negligible	<5% below 22 km 5–15% at 22–40 km
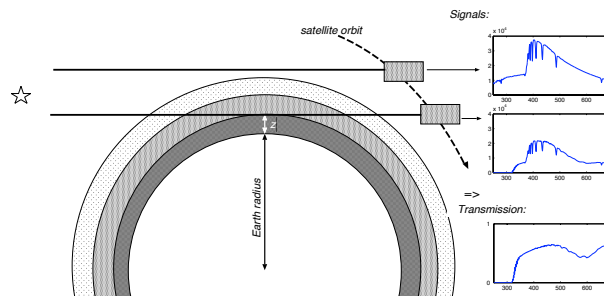
Fig. 1. The stellar occultation measurement principle of GOMOS. The horizontal transmission of the atmosphere is obtained by dividing the attenuated stellar spectrum with the reference spectrum measured above the atmosphere.
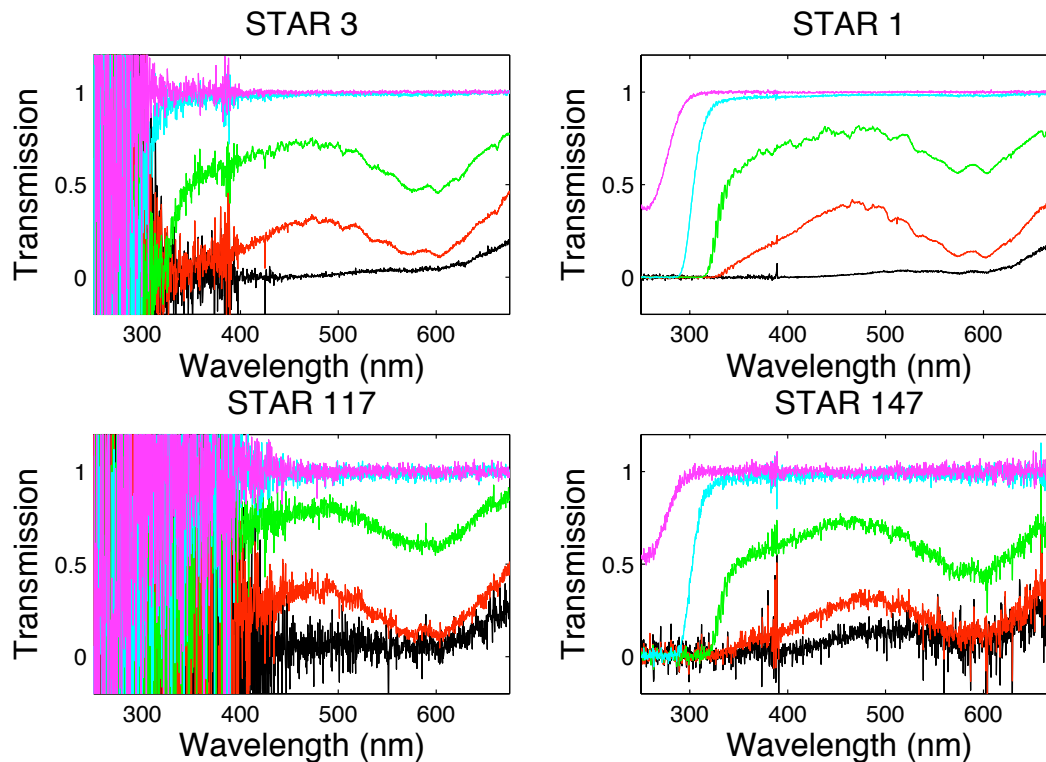
Fig. 2. Examples of GOMOS transmissions corrected for refractive effects measured using different stars, top row on left bright and cool star ($M_v = -0.05$, $T = 4300\,K$), on right bright and hot star ($M_v = -1.44$, $T = 11\,000\,K$), bottom row on left dim and cool star ($M_v = 2.7$, $T = 3800\,K$) and on right dim and hot star ($M_v = 2.88$, $T = 26\,000\,K$). Five lines correspond to altitudes 10 (black), 20 (red), 30 (green), 50 (cyan) and 70 km (magenta).
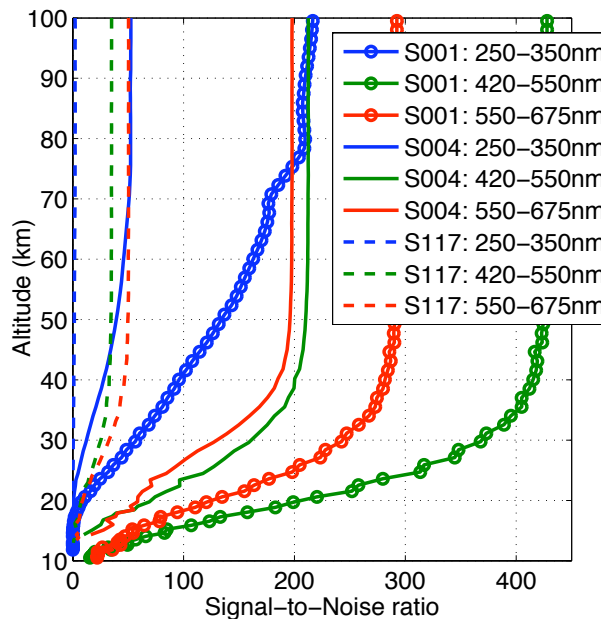
Fig. 3. The average signal-to-noise ratio for three stars as a function of altitude in 2003. Star 1, bright ($M_v = -1.44$) and hot star ($T = 11\,000$ K, solid line with circles) Star 4, bright and cool star ($M_v = -0.01$, $T = 5800$ K, solid line) and star 117, dim and cool star ($M_v = 2.7$, $T = 3800$ K, dashed line). Blue lines correspond to averaged SNR at UV: 250–350 nm, red line averaged SNR at VIS: 420–550 nm and green line averaged SNR at VIS: 550–675 nm.
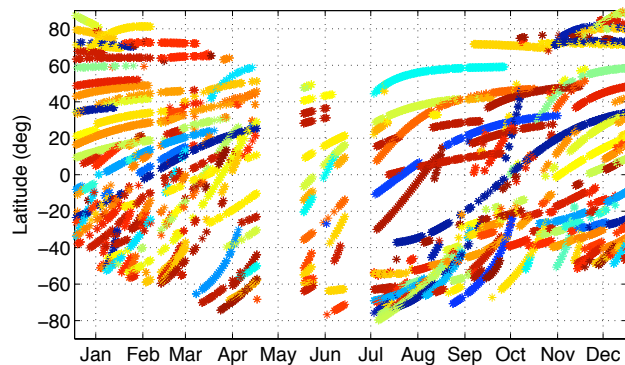
Fig. 4. Latitude coverage of GOMOS night measurements in 2003. The colours indicate the stellar brightness in magnitude. Dark blue indicates bright stars and red dim stars.
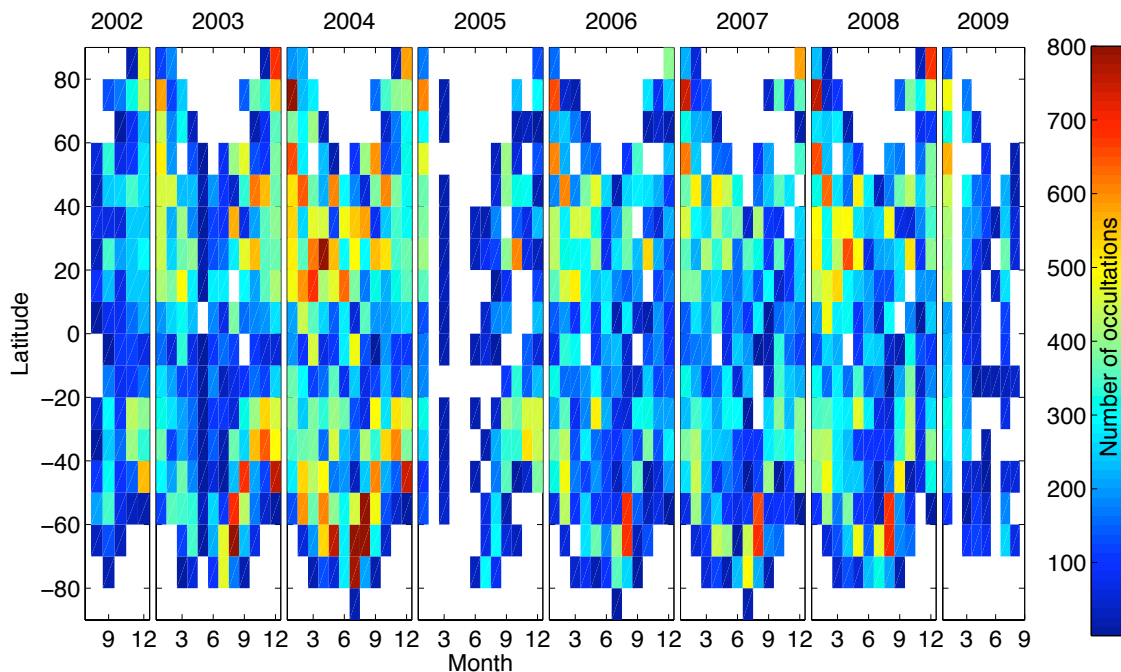
Fig. 5. Latitudinal distribution of GOMOS data availability during summer 2002–autumn 2009. Only night time data is considered here, i.e., solar zenith angle larger than 107 deg. Colour coding refers to number of available night time occultations.

Title Page

Abstract | Introduction

Conclusions | References

Tables | Figures

◄ | ►

Back | Close

Full Screen / Esc

Printer-friendly Version

Interactive Discussion
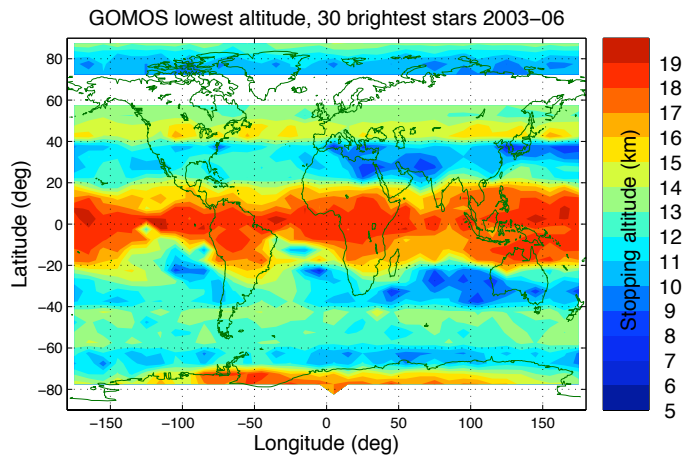
Fig. 6. Distribution of the mean occultation stopping altitude of 30 brightest stars in 2003–2006.
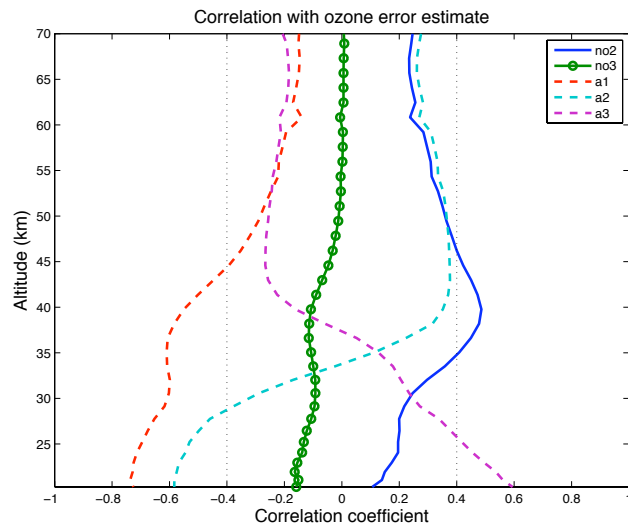
Fig. 7. Examples of correlation coefficients between the error estimates of horizontally integrated O_3 and NO_2 (solid blue line), NO_3 (green circles) and three aerosol parameters (dashed lines). Star 29 in tropics.
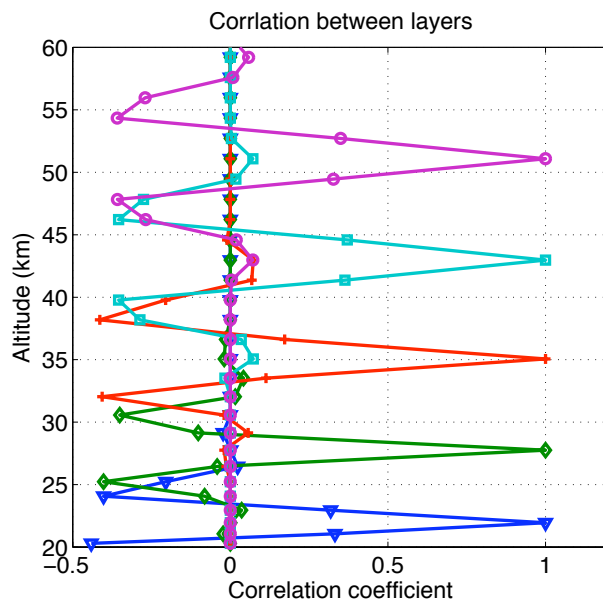
Fig. 8. Correlation of the retrieval error with neighbouring layers. Five selected altitudes (23, 28, 35, 34 and 51 km) are shown in different colours.
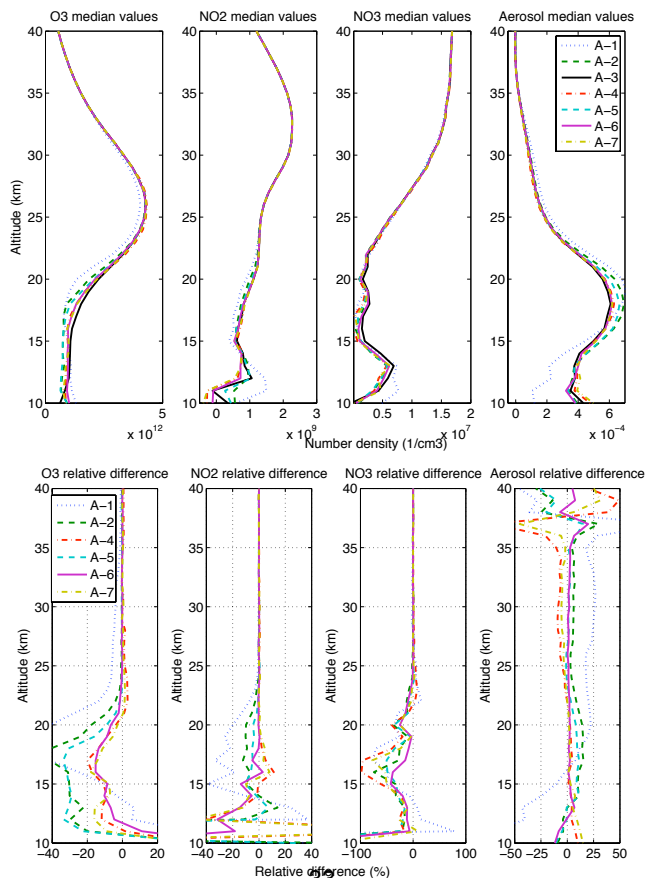
Fig. 9. Sensitivity of aerosol, O_3, NO_2 and NO_3 on selection of aerosol model. Seven aerosol models are compared (denoted with different line types and colours. Top row: median profiles and bottom row relative difference compared to second order polynomial model which is used in the operational GOMOS processing. From left: O_3, NO_2, NO_3 and aerosols. See text for the different aerosol models included.

Title Page

Abstract | Introduction

Conclusions | References

Tables | Figures

◄ | ►►

◄ | ►

Back | Close

Full Screen / Esc

Printer-friendly Version

Interactive Discussion
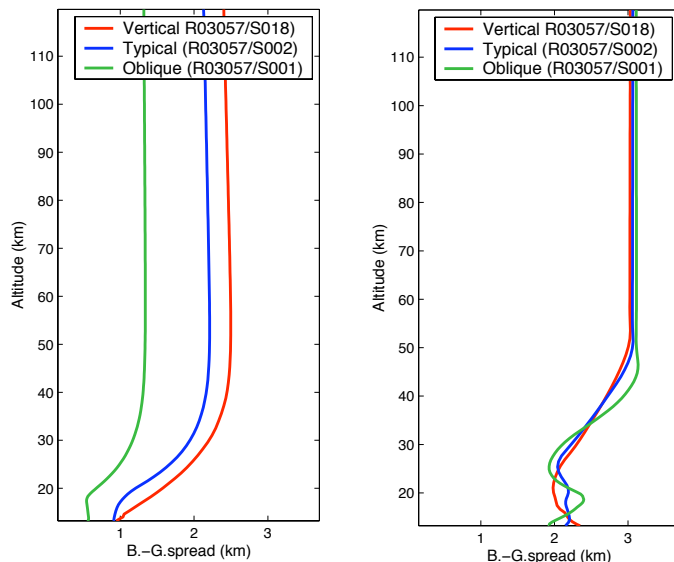
Fig. 10. Vertical resolution (Backus-Gilbert spread) of the ozone profiles in different occultation geometries as a function of altitude. On left: without regularizing, on right: with target resolution regularization. Red line denotes vertical occultation, blue line typical occultation and green line oblique occultation.
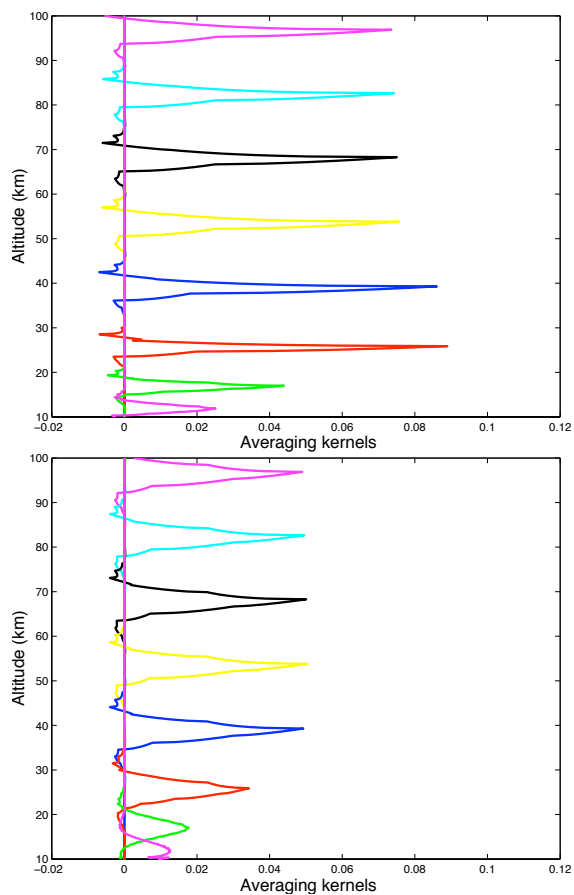
Fig. 11. Examples of averaging kernels. On left: ozone, on right: NO_2 and NO_3. Note that only every 10th averaging kernel is plotted.
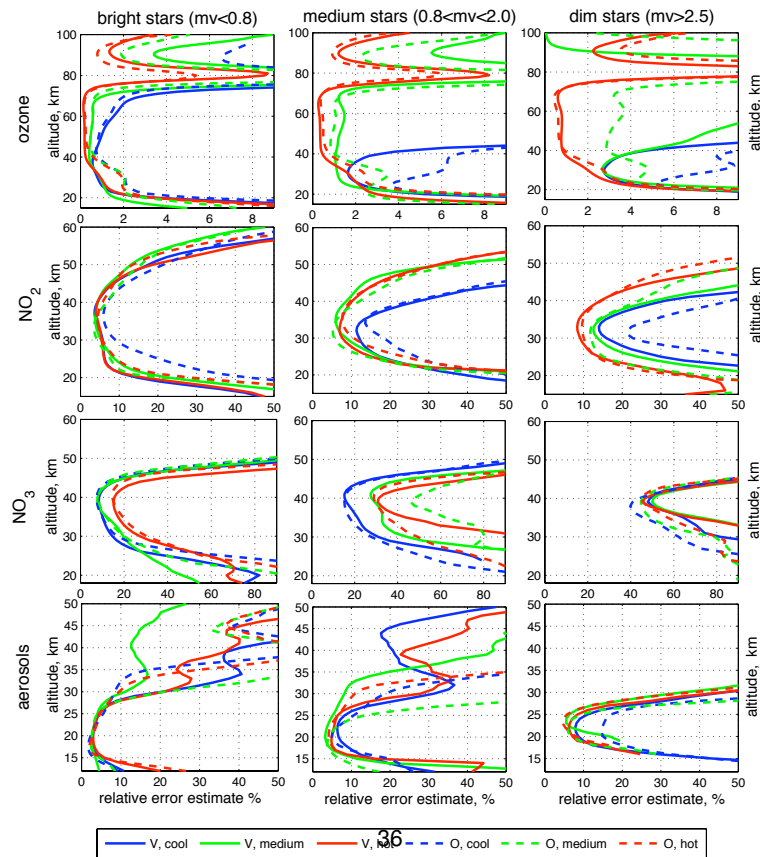
Fig. 12. GOMOS error estimates of O_3 (top row), NO_2 (second row), NO_3 (third row) and aerosols (bottom row) for representative cases: bright star (first column), typical star (middle column) and dim star (last column). The dashed lines correspond to oblique occultations and the solid lines to occultations in orbital plane. Stellar temperature is indicated with the line colour: hot stars (red), medium stars (green) and cool stars (blue). These values correspond to the upcoming data processing (IPF Version 6.0).

Title Page

Abstract | Introduction

Conclusions | References

Tables | Figures

◀ | ▶|

◀ | ▶

Back | Close

Full Screen / Esc
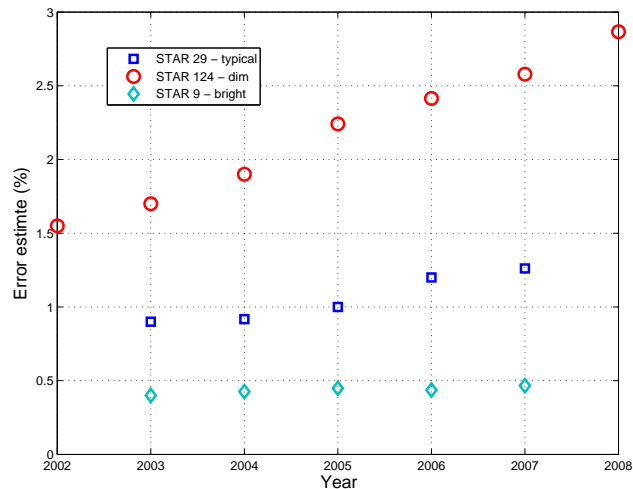
Printer-friendly Version

Interactive Discussion

Fig. 13. Averaged error estimates for three hot stars at 50 km as a function of time. Circle: Star number 9 (M_v=0.45, T=24 000 K), square: Star number 29 (M_v=1.7, T=10 200 K), diamond: star number 124 (M_v=2.7, T=26 000 K).